Regular Article

PHYSICAL CHEMISTRY RESEARCH
Published by the
Iranian Chemical Society
www.physchemres.org
info@physchemres.org

***Phys. Chem. Res.**, Vol. 5, No. 4, 795-817, December 2017*
DOI: 10.22036/pcr.2017.83153.1370

DFT Studies and Topological Analyses of Electron Density on Acetophenone and Propiophenone Thiosemicarbazone Derivatives as Covalent Inhibitors of Falcipain-2, a Major *Plasmodium Falciparum* Cysteine Protease

J. Numbonui Ghogomu* and N. Kennet Nkungli

Laboratory of Noxious Chemistry and Environmental Engineering, Department of Chemistry, Faculty of Science, University of Dschang, P.O. Box: 67, Dschang, Cameroon

(Received 25 April 2017, Accepted 26 August 2017)

Thiosemicarbazones (TSCs) possess significant antimalarial properties believed to be linked to the inhibition of major cysteine proteases, such as falcipain-2, in *Plasmodium falciparum*. However, the binding modes of TSCs to the active site of these enzymes are not clear. As a result of this, the nature of the bonding interactions between the active site of falcipain-2 and different derivatives of acetophenone thiosemicarbazone (APTSC) and propiophenone thiosemicarbazone (PPTSC) acting as inhibitors, have been studied herein *via* topological analyses of electron density. Derivatives of APTSC and PPTSC are well known to possess inhibitory effects against *Plasmodium falciparum*. Equilibrium geometries of the inhibitor-active site complexes in the aqueous phase have been obtained *via* dispersion-corrected density functional theory (DFT-D3) calculations. In-depth analyses of the covalent and noncovalent interactions in these complexes have been performed using the quantum theory of atoms in molecules (QTAIM) and the noncovalent interaction (NCI) index. Results have revealed a covalent interaction between the thiocarbonyl carbon of the TSC moiety and the thiolate sulfur of the active site cysteine residue of falcipain-2. Moreover, hydrogen bonding, dispersive-like van der Waals and π-stacking interactions have been elucidated between the TSC moiety of each inhibitor and the histidine residue of the enzyme's active site. The synergy of these interactions can enable the TSCs studied herein to specifically but transiently bind to the active site residues of falcipain-2. Based on our results, APTSC and PPTSC derivatives are potential reversible covalent inhibitors of falcipain-2, and are therefore promising precursors for the manufacture of antimalarial drugs.

Keywords: APTSC-PPTSC, Antimalaria, Falcipain-2, DFT, QTAIM, NCI

INTRODUCTION

Malaria is one of the most widespread parasitic diseases in the world [1,2], endemic in Sub-Saharan Africa and South-East Asia. This devastating disease is characterized by high morbidity and lethality [3], thus constituting a major public health problem. Significant efforts to fight against this disease have been made in the past years through the design and synthesis of quinoline-based antimalarial drug regimens and artemisinin-based combination therapies. Regrettably, the control of this disease has been hampered by the malaria parasites becoming increasingly resistant to the existing drugs [2]. Nevertheless, the search for novel and more effective antimalarial drugs is ongoing. Thiosemicarbazones (TSCs) are among the potential new antimalarial agents which have been extensively investigated for their antiplasmodial activities. Interestingly, TSCs display a wide spectrum of pharmacological properties including antimalarial activities [4,5]. Consequently, TSCs can be exploited in the development of new antimalarial drugs [1]. Recently, the TSCs: 3,4-dichloroacetophenone thiosemicarbazone (DAPTSC) and 3,4-dichloropropiophenone thiosemicarbazone (DPPTSC) have been synthesized and found to possess antiplasmodial

*Corresponding author. E-mail: ghogsjuju@hotmail.com

effects against chloroquine-resistant and chloroquine-sensitive *Plasmodium falciparum* strains [6,7]. However, a major drawback of TSCs as antimalarial agents is that their precise antiplasmodial mechanism is currently not clear. It is believed that their antimalarial activity is due to the inhibition of cysteine protease enzymes present in *Plasmodium falciparum* (*P. falciparum*) and *Plasmodium vivax* (*P. vivax*), known as falcipains and vivapains, respectively [1,4,8]. These enzymes are required for several parasitic functions in *P. falciparum* and *P. vivax*, especially the degradation of the host hemoglobin [7,9]. The inhibition of cysteine proteases by TSCs has been supported by the findings of a study carried out by Trossini and co-workers [10] on cruzain, a major cysteine protease from *Trypanosoma cruzi*.

Although the antimalarial effects of DAPTSC and DPPTSC are linked to the inhibition of key cysteine proteases in *P. falciparum* [7], the nature of the interactions between TSCs and the active site of these enzymes remains unclear. Therefore, further studies to identify and classify the covalent and/or noncovalent interactions between the active site of falcipains and each of the TSCs DAPTSC and DPPTSC are warranted. In this regard, the present work is geared toward elucidating the binding modes of TSC-based inhibitors to the active site of the cysteine proteases found in malaria parasites, using falcipain-2 (FP2) as an illustrative example. Falcipains have been chosen because of their key role in the parasitic activities of the most virulent human malaria parasite, *P. falciparum*. FP2 is typically localized in the acidic food vacuoles of erythrocytic *P. falciparum* parasites, where it degrades the host hemoglobin to supply the amino acids required for their growth and development [2,11]. The possible covalent and noncovalent interactions between TSCs and the active site of FP2 can be robustly elucidated by topological analysis of the electron density distributions of TSC-FP2 active site complexes. In the realm of theoretical chemistry, suitable electron density distributions of these complexes can be obtained from long-range dispersion corrected density functional theory (DFT-D3) calculations [12,13]. It is worthy of note that DAPTSC and DPPTSC can act as covalent reversible inhibitors of falcipains initiated by a nucleophilic attack by the thiolate sulfur of the active site cysteine residue on electrophilic centers in the TSC moiety such as the thione carbon and/or imine carbon [7,10].

Another important TSC known as 4-methoxy-acetophenone thiosemicarbazone (MAPTSC), a derivative of acetophenone thiosemicarbazone, has been synthesized and found to have inhibitory effects against *Trypanosoma brucei brucei* [4], which is a parasite that depends on cysteine proteases for many life-sustaining biochemical processes [14]. Hence, MAPTSC and 4-methoxy-propiophenone thiosemicarbazone (MPPTSC), like DAPTSC and DPPTSC are likely to possess antiplasmodial effects based on cysteine protease inhibition. Herein, theoretical calculations aimed at elucidating the covalent and noncovalent interactions between the active site residues of FP2 (Cysteine-25 and Histidine-159, see Fig. 1) and each of the TSCs; MAPTSC, MPPTSC, DAPTSC and DPPTSC (acting as inhibitors) have been carried out using the quantum mechanical (QM)-cluster approach. The DFT-D3 quantum chemical method and the electron density topological methods: quantum theory of atoms in molecules (QTAIM) and the noncovalent interaction (NCI) index have been employed. An in-depth analysis of the bonding interactions between the active site residues of FP2 and these molecules has been performed in order to provide detailed insight into the cysteine protease inhibition process by TSCs. Interestingly, strong inhibition of FP2 would severely compromise the hemoglobin degradation process that is paramount for the survival of *P. falciparum* [7,8]. An active site is found in the molecular structure of FP2 (shown in Fig. 1), comprised of a free cysteine residue (Cys-25), which acts in concert with a proximal histidine residue (His-159) [14].

COMPUTATIONAL DETAILS AND THE QUANTUM MECHANICAL (QM)-CLUSTERS ADOPTED

All DFT calculations have been performed with the ORCA 3.0.3 software package [15]. The restricted Kohn-Sham model has been adopted in all calculations because the molecules studied are all closed shell systems. The structural model of the active site of FP2 used in this study was extracted from the enzyme's crystal structure rendered from the PDB file 1YVB (see Fig. 1), using VMD 1.9.3 [16]. Although the active site of falcipains consists of a

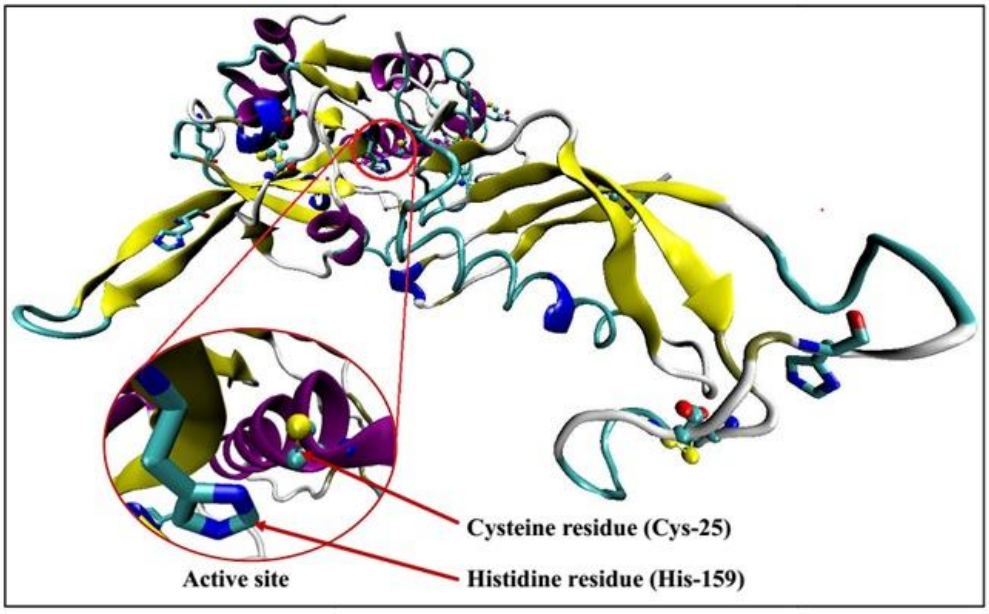

Fig. 1. Structure of the *Plasmodium falciparum* cysteine protease falcipain-2, rendered from the protein data bank (PDB) file ID: 1YVB.

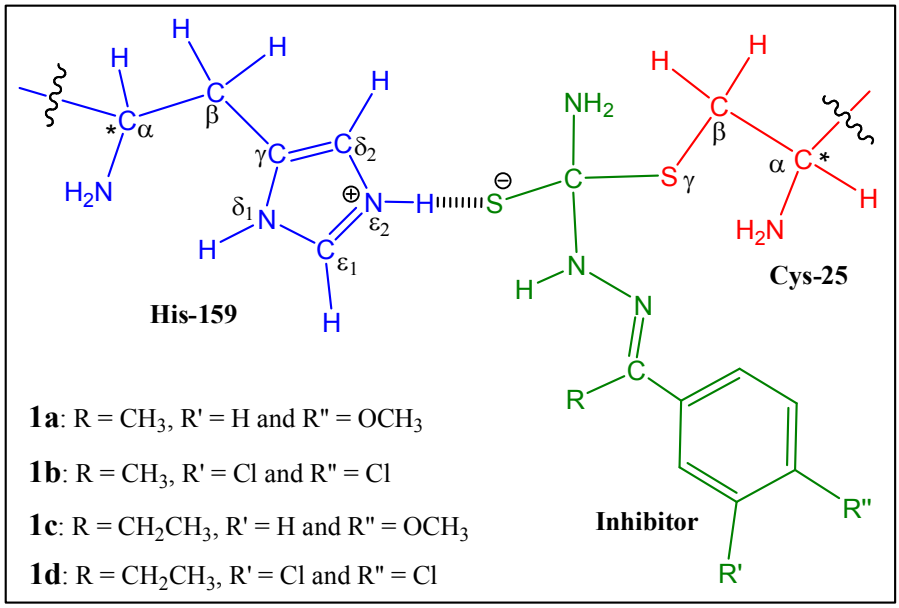

Fig. 2. The QM-clusters for the inhibitor-active site complexes studied (1a, 1b, 1c and 1d) comprising of the inhibitor molecule (green), the Cys-25 residue (red) and the His-159 residue (blue), interconnected *via* covalent and H-bond interactions. The atoms marked with asterisks (alpha-carbons of Cys-25 and His-159 linked to the protein backbone) were held constant during geometry optimization.

catalytic triad comprising asparagine (Asn-175), cysteine (Cys-25) and histidine (His-159) residues, their catalytic activity is solely dependent on the Cys-25 and His-159 residues [8,17]. The role of Asn-175 is to maintain the imidazole ring of His-159 in a favorable orientation and proximity to Cys-25 [17]. The QM-cluster for each inhibitor-active site complex investigated comprises the inhibitor molecule attached to deprotonated Cys-25 residue, *via* a covalent bond between the thiolate sulfur of Cys-25 and the thiocarbonyl carbon of the inhibitor's TSC moiety, assisted by an H-bond interaction between the sulfur atom of the TSC moiety and the hydrogen atom attached to the epsilon-nitrogen (ε_2) of protonated His-159 residue, as illustrated in Fig. 2. The complexes investigated are: [(Cys-25···His-159)(MAPTSC)] (1a), [(Cys-25···His-159)(DAPTSC)] (1b), [(Cys-25···His-159)(MPPTSC)] (1c) and [(Cys-25···His-159)(DPPTSC)] (1d). In this paper, the foregoing complexes are described as series 1. Also studied herein, is a second series of complexes denoted 2a, 2b, 2c and 2d, which differ from the complexes 1a-1d (series 1) in that the hydrogen atom attached to the epsilon-nitrogen (ε_2) of the protonated His-159 residue is abstracted by the sulfur atom of the TSC moiety.

The geometries of the inhibitor molecules were optimized at RI-BP86-D3(BJ)/def2-TZVP level of theory without constraints of any kind. The BP86 functional [18,19] was chosen because it predicts excellent geometries and vibrational frequencies [12]. To ensure effective geometry optimization, this functional was employed along with the triple-zeta polarized basis set def2-TZVP. In order to incorporate long-range dispersion interaction effects, the latest available Grimme's atom pair-wise dispersion correction using the Becke-Johnson damping scheme [D3(BJ)] [20] was employed in our calculations. The inhibitor-active site complexes studied were optimized at the same level of theory as that used in optimizing the free inhibitor molecules, using the fragment optimization approach implemented in ORCA 3.0.3. By this approach, each inhibitor molecule and the deprotonated Cys-25 residue were treated as fragment 1, while the protonated His-159 residue was considered as fragment 2. In order not to compromise the structural integrity of the enzyme's active site due to the omission of the protein backbone in Fig. 2, the Cartesian coordinates of the alpha-carbons of Cys-25 and His-159 linked to this protein backbone were held constant during geometry optimization. For the same reason, a similar constraint was implemented during the geometry optimization of the isolated active site model of FP2 as extracted from the PDB file 1YVB. In the complexes investigated, the geometries of the inhibitor molecules along with those of the Cys-25 and His-159 residues of the active site were relaxed in order to account for any structural adjustments resulting from inhibitor-active site binding.

Topological analyses of electron density have been performed on the BP86-D3 optimized geometries of the inhibitor-active site complexes studied, within the framework of QTAIM using the AIMAll program package [21]. On the other hand, the NCI index analyses were performed using the Multiwfn 3.3.9 software [22]. In all cases, topological analyses of electron density have been performed using wavefunction files obtained from single-point calculations at RIJCOSX-M06-2X/def2-TZVPP level of theory. The molecular graphs of the various inhibitor-active site complexes were generated using Avogadro 1.1.1 [23], based on ORCA/molden2aim-generated wavefunction (WFN) files. The NCI isosurfaces of the complexes were plotted using the VMD 1.9.3 software [16] based on Multiwfn-generated Gaussian cube files.

For all theoretical calculations performed in this work, solvent effects were modeled by the SMD continuum solvation model [24] as implemented in ORCA 3.0.3. Water was chosen as solvent in order to simulate the aqueous environment in living organisms. The resolution-of-the-identity (RI-J) approximation [25] was used in synergy with the chain-of-spheres (COSX) approximation [26], along with suitable auxiliary basis sets to speed-up calculations. The loss of accuracy that arises from the use of the RI-J or RIJCOSX approximations is negligible [27]. To ascertain that the optimized geometries are minima on their potential energy surfaces (PES), vibrational frequencies were calculated at the same level of theory as that used for the geometry optimizations. No imaginary frequencies were obtained, confirming all optimized geometries as minima

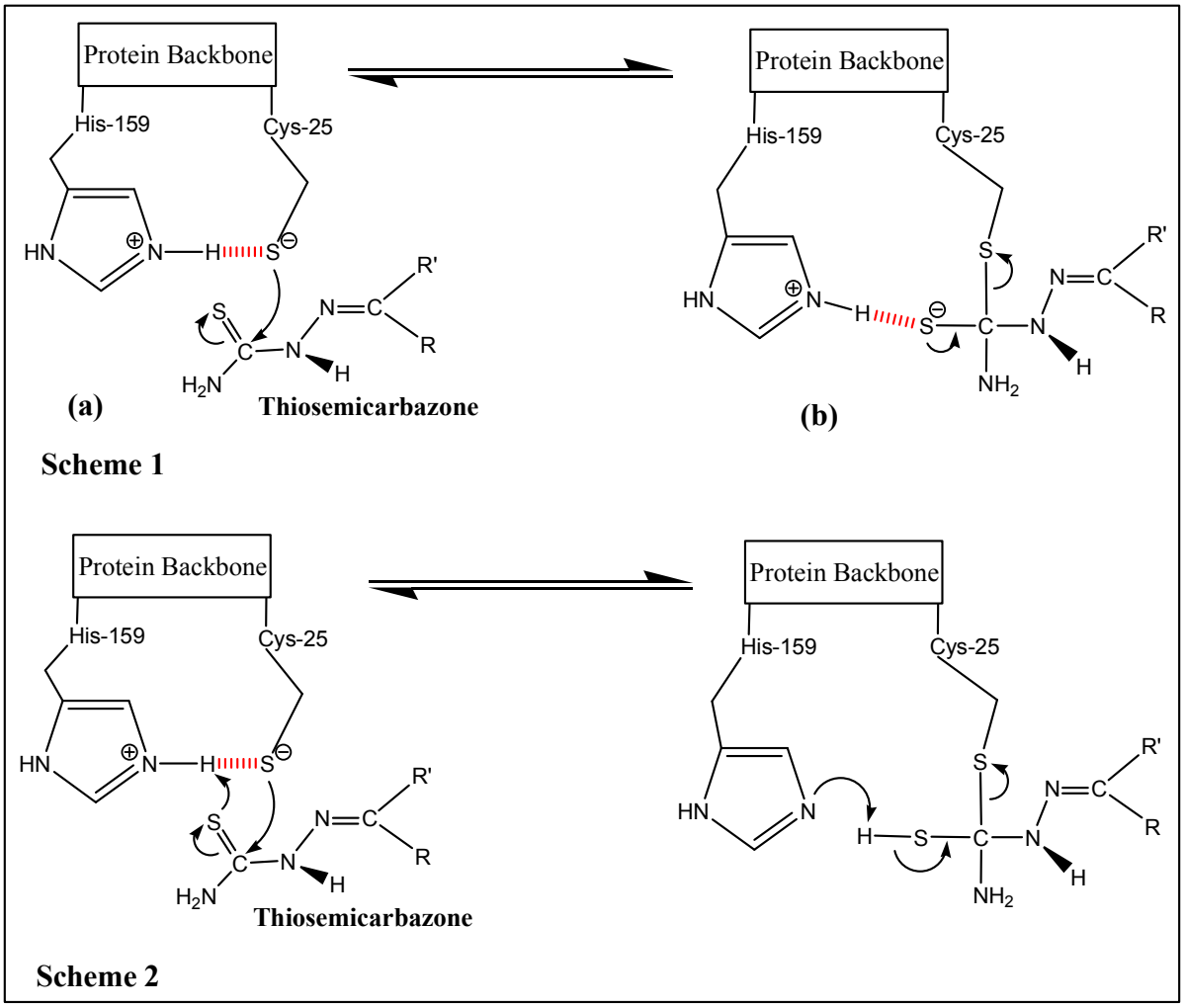

Fig. 3. Proposed inhibition mechanism of falcipains by TSC-based inhibitors. 3(a): thiolate sulfur of thiolate-Imidazolium ion pair attacks to a TSC-based inhibitor; 3(b): inhibitor tightly bound by covalent and hydrogen bonding interactions to enzyme's active site.

on their respective PES.

RESULTS AND DISCUSSIONS

Proposed Inhibition Mechanism of Falcipains by TSC-based Inhibitors

The active site of falcipains and other cysteine proteases is located in a groove found on the surface of the enzymes [9]. The Cys-25 residue of the cysteine protease active site is usually deprotonated to a thiolate anion by the active site His-159 residue, which in turn is protonated at the epsilon-nitrogen of the imidazole ring to an imidazolium cation. Consequently, a stable thiolate-imidazolium ion pair is formed at the active site of the enzyme as shown in Scheme 1a of Fig. 3 [14,28]. To catalyze protein degradation, a cysteine protease enzyme such as FP2 binds onto the protein substrate *via* a nucleophilic attack by the thiolate sulfur of the deprotonated active site Cys-25 residue, on a carbonyl carbon of the peptide. This eventually leads to the cleavage

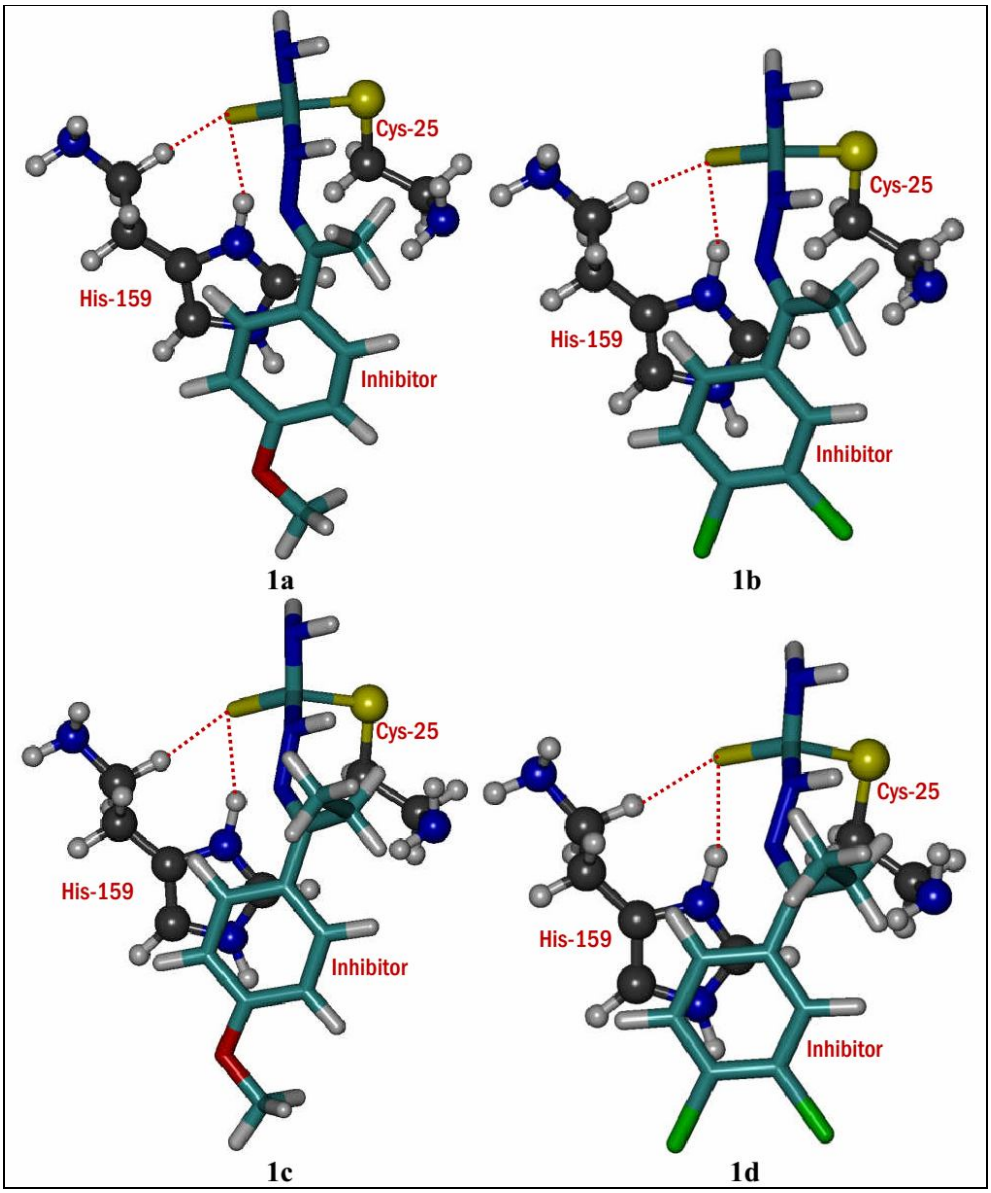

Fig. 4. Optimized geometries of the complexes of series 1, visualized using VMD 1.9.3. In each complex, the active site Cys-25 and His-159 residues are represented with balls and sticks, while the inhibitor molecules are represented only with sticks. The carbon skeletons of Cys-25 and His-159 are gray, while those of the inhibitors are cyan colored. H-bonds are shown by the red colored dashed lines.

of the peptide and the regeneration of the active site [14]. In this paper, it is hypothesized that the inhibition mechanism of falcipains (using FP2 as an illustrative example) by acetophenone and propiophenone TSC derivatives is as shown in Scheme 1 of Fig. 3, based on the reactivity of the TSC sulfur with cysteines as envisaged in [10]. These TSCs can inhibit FP2 through the formation of a covalent linkage between the thiocarbonyl carbon of the TSC moiety and the thiolate sulfur of the active site Cys-25 residue. The formation of this covalent bond is mediated by a

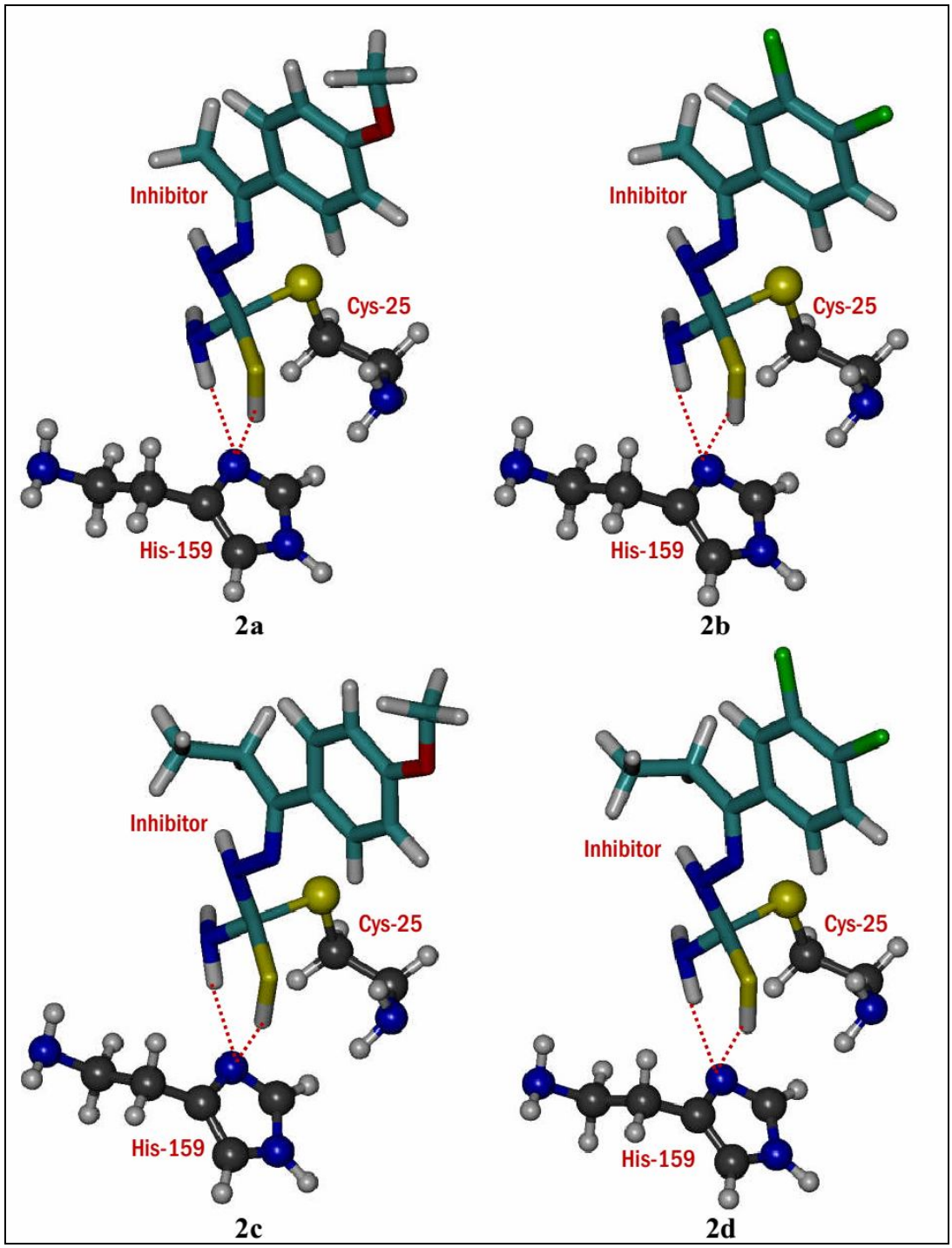

Fig. 5. Optimized geometries of the complexes of series 2, visualized using VMD 1.9.3. In each complex, the active site Cys-25 and His-159 residues are represented with balls and sticks, while the inhibitor molecules are represented only with sticks. The carbon skeletons of Cys-25 and His-159 are gray, while those of the inhibitors are cyan colored. H-bonds are shown by the red colored dashed lines.

Table 1. The Different Types of Intermolecular Interactions in the Inhibitor-FP2 Active Site Complexes Investigated, Along with their Bond Lengths and Angles

Series 1 complexes	Intermolecular interaction	Interaction type	C-H/N-H/C-S bond length (Å)	H···S bond length (Å)	C-H···S/N-H···S bond angle (°)
1a	C45-H50···S5	H-bond	1.100	2.827	132.0
	N39-H56···S5	H-bond	1.067	2.118	163.2
	C3-S29	Covalent bond	1.952	-	-
	Phenyl ring-Imidazole ring	π-stacking	-	-	-
1b	C41-H46···S5	H-bond	1.100	2.829	131.7
	N35-H52···S5	H-bond	1.069	2.111	163.8
	C3-S25	Covalent bond	1.946	-	-
	Phenyl ring-Imidazole ring	π-stacking	-	-	-
1c	C48-H53···S5	H-bond	1.100	2.821	131.6
	N42-H59···S5	H-bond	1.067	2.118	163.0
	C3-S32	Covalent bond	1.953	-	-
	Phenyl ring-Imidazole ring	π-stacking	-	-	-
1d	C44-H49···S5	H-bond	1.100	2.826	131.7
	N38-H55···S5	H-bond	1.069	2.106	163.8
	C3-S28	Covalent bond	1.946	-	-
	Phenyl ring-Imidazole ring	π-stacking	-	-	-
Series 2 complexes	Intermolecular interaction	Interaction type	S-H/N-H/C-S bond length (Å)	H···N bond length (Å)	S-H···N/N-H···N bond angle (°)
2a	S5-H29···N40	H-bond	1.357	2.269	158.6
	N4-H27···N40	H-bond	1.032	2.074	170.5
	C3-S30	Covalent bond	1.920	-	-

Table 1. Continued

2b	S5-H25···N36	H-bond	1.357	2.260	158.2
	N4-H23···N36	H-bond	1.033	2.068	170.6
	C3-S26	Covalent bond	1.918	-	-
2c	S5-H32···N43	H-bond	1.357	2.271	158.9
	N4-H30···N43	H-bond	1.032	2.074	170.5
	C3-S33	Covalent bond	1.921	-	-
2d	S5-H28···N39	H-bond	1.357	2.263	158.6
	N4-H26···N39	H-bond	1.033	2.069	170.6
	C3-S29	Covalent bond	1.918	-	-

nucleophilic attack undergone by the thiolate sulfur of the deprotonated active site Cys-25 residue on the thiocarbonyl carbon of the TSC moiety. This is immediately followed by an electron pair transfer to the thiocarbonyl sulfur of the TSC moiety, which is then transformed into a thiolate anion. The negatively charged adduct formed is stabilized by an H-bond interaction between the hydrogen atom attached to the epsilon-nitrogen of the imidazole ring in the positively charged protonated His-159 residue, and the thiolate sulfur of the TSC moiety, as shown in Scheme 1b of Fig. 3.

The mechanism of cysteine protease inhibition by acetophenone and propiophenone TSC derivatives proposed in this work (Scheme 1 of Fig. 3), like that suggested in [10] (Scheme 2 of Fig. 3) is apparently reversible. Based on the foregoing ideas, acetophenone and propiophenone TSC derivatives are potential reversible covalent inhibitors of falcipains. Although the main aim of this work is to determine the binding modes of the TSC-based inhibitors to the FP2 active site residues, an attempt has been made to determine the most preferred inhibition mechanism between that proposed in the present work and the one suggested in [10]. In this regard, the relative stability of the complexes: 1a-1d (series 1) and 2a-2d (series 2) obtained from Schemes 1 and 2 respectively, has been investigated based on electronic energy and thermochemical analysis, since the most preferred mechanism is likely that which yields the most stable complexes. Thereafter, the nature of the covalent and noncovalent interactions between each inhibitor molecule and the FP2 active site in these complexes have been scrutinized in the following sections, using methods based on topological analysis of electron density.

Structural and Relative Stability Analyses

The geometries of all inhibitor-FP2 active site complexes investigated herein (optimized at RI-BP86-D3(BJ)/def2-TZVP level of theory) are depicted in Figs. 4 and 5. The types of intermolecular interactions in these complexes, along with their bond lengths and angles are listed in Table 1. The H-bonds described in Table 1 were identified using geometrical cutoff limits proposed by Jeffrey [29], along with the van der Waal radii cutoff limit for H-bond formation.

It is clear from Fig. 4 that a thiolate sulfur (S^-) of the TSC moiety acts as an H-bond acceptor in the complexes of series 1 (1a-1d), whereas in the complexes of series 2 (see Fig. 5), a thiol group (S-H) of the TSC moiety acts as an H-bond donor. Indeed, sulfur in the form of a thiolate anion is a potential H-bond acceptor, and as part of the S-H group is a very good H-bond donor [30]. Research on protein cysteine sulfurs has shown that in H-bond interactions of the type S-H···A (where the S-H group is the donor and A is the acceptor), the average H-bond lengths are in the range 2.51-2.84 Å depending on the nature of A, whereas in H-bond

interactions of the type X-H···S (where S^- is the acceptor and X-H is the donor), the average H-bond length can be up to 2.80 Å [31]. In the present study, the bond lengths of all H-bond interactions of the type S-H···N (only found in complexes of series 2) are in the range 2.260-2.271 Å, while those of all H-bond interactions of the types C-H···S and N-H···S (only found in complexes of series 1) are in the range 2.106-2.829 Å. Hence, the calculated bond lengths of all sulfur-centered H-bonds in this work are in good agreement with those reported in [31], indicating the validity of the optimized geometries of the complexes studied herein.

Apart from the covalent bond between the thiocarbonyl carbon and the thiolate sulfur of the Cys-25 residue, the complexes 1a-1d (series 1) are each stabilized by intermolecular H-bonds of the type C-H···S and N-H···S, while each of the complexes 2a-2d (series 2) is stabilized by intermolecular H-bonds of the type S-H···N and N-H···N. In the light of Jeffrey's categorization of H-bonds [29], the non-conventional H-bonds: C45-H50···S5, C41-H46···S5, C48-H53···S5 and C44-H49···S5 in the complexes 1a, 1b, 1c and 1d, respectively, are found to be weak and dispersive in nature. This conclusion has been drawn based on the following facts: the H-bond length H···S > 2.2 Å, the bond length C-H is far less than the H-bond length H···S [29], and the bond angles C-H···S are in the range 90°-150° [32], in all cases. Still based on the classification of H-bonds by Jeffery, the rest of the intermolecular H-bonds in 1a-1d, along with all intermolecular H-bonds in 2a-2d are found to be moderately strong and mostly electrostatic in nature. The H-bond interactions reported in Table 1 have been validated on the basis of the van der Waal cutoff limit for H-bond formation, which requires that the H···A distance be substantially shorter than the sum of the van der Waals radii of H and A (where A is the H-bond acceptor) [33]. Interestingly, the H-bond lengths H···S (2.106-2.829 Å) and H···N (2.068-2.271 Å) are shorter than the sum of the van der Waals radii of H and S (3.00 Å), and of H and N (2.75 Å), respectively, for all H-bonds listed in Table 1.

In complexes of both series 1 and 2, the synergy of the intermolecular H-bonds and the covalent bond between the thiolate sulfur of Cys-25 and the thiocarbonyl carbon of the TSC moiety can enable each of the TSC-based inhibitors to bind specifically but transiently to the active site residues of FP2. It can be seen from Fig. 4 that in addition to the intermolecular H-bonds and the covalent bond in complexes of both series 1 and 2, π-stacking is also a prominent feature in all complexes of series 1 (1a-1d). In these complexes, the phenyl ring in each inhibitor molecule is apparently in a position favorable for π-stacking interaction with the imidazole ring of His-159. Since π-stacking interactions are highly non-directional, values of bond lengths and angles are not available for these interactions in 1a-1d. The stabilizing role played by these π-stacking interactions is one of the key reasons for the extra stability of the complexes of series 1 relative to those of series 2 as discussed below.

The relative stability of the BP86-D3 optimized geometries of the complexes of both series 1 and series 2 has been investigated based on the calculated electronic energies and thermodynamic parameters (enthalpy and Gibbs free energy of formation). Besides the relative stability studies, the electronic energies (*E*) of the complexes investigated have been calculated at two different theoretical levels: RIJCOSX-M06-2X/def2-TZVPP and RIJCOSX-B3LYP-D3(BJ)/def2-TZVPP for comparison, in an effort to choose between the Minnesota functional M06-2X [34] and the popular hybrid functional B3LYP [35,36] augmented with the latest Grimme's dispersion correction term D3, a more appropriate DFT functional for further analysis. On the other hand, the standard enthalpy (H_f°) and Gibbs free energy (G_f°) of formation of these complexes have been computed *via* thermochemical analysis at RI-BP86-D3(BJ)/def2-TZVP level of theory. The relative values: ΔE, ΔH_f° and ΔG_f° listed in Table 2 were calculated by subtracting the corresponding parameters of the complexes 2a, 2b, 2c and 2d from those of all complexes studied. For instance, the ΔE values; -4.426 kcal mol^{-1} for 1a and 0.000 kcal mol^{-1} for 2a were calculated from $\Delta E = E_{1a} - E_{2a}$ and $\Delta E = E_{2a} - E_{2a}$, respectively.

The electronic energies, enthalpies and Gibbs free energies of all complexes currently investigated indicate that the complexes 1a-1d are more stable than the corresponding 2a-2d series. The small values of ΔE, ΔH_f° and ΔG_f° are indicative of the likelihood of the mechanism of cysteine protease inhibition (proposed herein) occurring

Table 2. Electronic Energies and Thermodynamic Parameters of the Complexes Investigated

Complex	M06-2X/def2-TZVPP	B3LYP-D3/def2-TZVPP	BP86-D3/def2-TZVP	
	ΔE (kcal mol^{-1})	ΔE (kcal mol^{-1})	ΔH_f° (kcal mol^{-1})	ΔG_f° (kcal mol^{-1})
1a	-4.426	-4.654	-3.083	-5.389
2a	0.000	0.000	0.000	0.000
1b	-4.502	-4.943	-4.066	-4.132
2b	0.000	0.000	0.000	0.000
1c	-4.569	-4.816	-3.612	-4.408
2c	0.000	0.000	0.000	0.000
1d	-4.299	-4.789	-3.841	-4.293
2d	0.000	0.000	0.000	0.000

concomitantly with that suggested in [10], with the former mechanism being slightly more preferable than the latter. It is also clear from Table 2 that the electronic energies computed using M06-2X in conjunction with the basis set def2-TZVPP, are lower than those computed using B3LYP-D3 in conjunction with the same basis set. A possible reason for this discrepancy is that the former functional is more effective in describing the noncovalent interactions in these complexes. In fact, the M06-2X functional is recommended for applications involving main-group thermochemistry and noncovalent interactions [34]. Consequently, further theoretical calculations and analyses in this paper pertaining to noncovalent interactions were performed using the M06-2X functional.

Quantum Theory of Atoms in Molecules (QTAIM) Analysis

In order to critically analyze the geometries and noncovalent interactions in the inhibitor-FP2 active site complexes currently studied, topological analyses of their electron density distributions were carried out within the framework of Bader's quantum theory of atoms in molecules (QTAIM) [37]. Indeed, QTAIM is a very popular and useful methodology for investigating the covalent and noncovalent interactions in molecular systems. Such interactions in the complexes studied, particularly those between the inhibitor molecules and the FP2 active site, have been identified and classified using criteria based on the topological properties of electron density at bond critical points (BCPs). In this study, the topological properties at the BCPs were described and classified in terms of the following parameters: the electron density ($\rho(r_{BCP})$), the Laplacian of electron density ($\nabla^2\rho(r_{BCP})$), the Lagrangian kinetic energy density ($G(r_{BCP})$), the potential energy density ($V(r_{BCP})$) and the energy density ($H(r_{BCP})$).

Generally, $\rho(r_{BCP})$ is greater than 0.20 a.u. in shared (covalent) bonding and less than 0.10 a.u. in closed-shell interactions (for example ionic, van der Waals, hydrogen, dihydrogen, H-H bonding, *etc.*) [38-40]. The sign of

$\nabla^2\rho(r_{BCP})$ reveals whether electron density is largely concentrated in the interatomic space as in covalent bonds ($\nabla^2\rho(r_{BCP}) < 0$), or depleted as in closed-shell (electrostatic) interactions ($\nabla^2\rho(r_{BCP}) > 0$) [40,41]. The energy density given by $H(r) = G(r) + V(r)$ has been used by Cremer and Kraka [42] to classify bonded interactions because it effectively distinguishes between covalent bonds and closed-shell interactions. Generally, $H(r_{BCP}) < 0$ is typical of a covalent bond, while $H(r_{BCP}) > 0$ is indicative of a closed-shell interaction. Interestingly, the values of $H(r_{BCP})$ and $\nabla^2\rho(r_{BCP})$ in the bonding region can be used as a measure of the type and strength of a covalent bond: $\nabla^2\rho(r_{BCP}) > 0$ and $H(r_{BCP}) > 0$ indicate closed-shell (electrostatic) interactions, $\nabla^2\rho(r_{BCP}) < 0$ and $H(r_{BCP}) < 0$ indicate covalent interactions, and $\nabla^2\rho(r_{BCP}) > 0$ and $H(r_{BCP}) < 0$ indicate partial covalent interactions [43]. Another useful descriptor of chemical bonds is the $-V(r_{BCP})/G(r_{BCP})$ ratio, while $-V(r_{BCP})/G(r_{BCP}) < 1$ is characteristic of a typical ionic bond, $-V(r_{BCP})/G(r_{BCP}) > 2$ is diagnostic of a classical covalent interaction [44].

In the QTAIM framework, Koch and Popelier [45] proposed three criteria for the existence of an H-bond: (1) the H-bond must be accompanied by a BCP, (2) the value of $\rho(r)$ should fall within 0.002-0.040 a.u., and (3) the $\nabla^2\rho(r_{BCP})$ value should be positive and within 0.024-0.139 a.u. Moreover, the nature of H-bonds have been evaluated based on their interatomic interaction energies (E_{int}) estimated by the Espinosa approach, Eq. (1) [46]. Typical H-bond energies are in the range 3-10 kcal mol^{-1} [29,33].

$$E_{int}(a.u.) = \frac{1}{2}V(r_{BCP}) \quad (1)$$

All QTAIM calculations have been carried out at RIJCOSX-M06-2X/def2-TZVPP level of theory, and the results are presented in Tables 3 and 4 for complexes of series 1 and 2, respectively. The corresponding molecular graphs of these series of complexes, plotted using Avogadro 1.1.1 [23], are displayed in Figs. 6 and 7, respectively. Among the intermolecular interactions within each inhibitor-FP2 active site complex, only those found between the TSC-based inhibitor molecules and the active site residues of FP2 are listed in Tables 3 and 4, and are also labeled in Figs. 6 and 7, since they are undoubtedly the interactions responsible for the binding of the inhibitor and the active site. In all cases studied, $\nabla^2\rho(r_{BCP}) < 0$ and $H(r_{BCP}) < 0$ for the interactions: C3-S29, C3-S25, C3-S32, C3-S28, C3-S30, C3-S26, C3-S33 and C3-S29 between the thiocarbonyl carbon of each TSC-based inhibitor and the thiolate sulfur of the deprotonated Cys-25 active site residue, showing that in each inhibitor-FP2 active site complex, the interaction is a covalent bond. The covalent nature of these interactions is further confirmed by the ratio $-V(r_{BCP})/G(r_{BCP}) > 2$ in all cases, coupled with their large interaction energies ranging from -27.403 to -28.085 kcal mol^{-1}. In all complexes studied, $\nabla^2\rho(r_{BCP}) > 0$ and $H(r_{BCP}) < 0$ for each H-bond of the form: N-H···S, S-H···N and N-H···N, which indicate that they are closed-shell but partially covalent interactions. The rest of the interactions in these complexes as listed in Tables 3 and 4 are closed-shell electrostatic interactions, since $\nabla^2\rho(r_{BCP}) > 0$ and $H(r_{BCP}) > 0$ in each case. The closed-shell character of these interactions is further validated by the fact that their $\rho(r_{BCP})$ values are less than 0.10 a.u. Interestingly, all H-bonds in the complexes investigated have clearly satisfied the three criteria for the existence of an H-bond proposed by Koch and Popelier [45].

In each of the complexes 1a-1d, QTAIM analysis has revealed a strong H-bond of the form N-H···S (with $\rho(r_{BCP}) \simeq 0.035$ a.u., an average E_{int} value -7.685 kcal mol^{-1} and $1 < -V(r_{BCP})/G(r_{BCP}) < 2$) between the hydrogen atom attached to the epsilon-nitrogen of the imidazole ring in protonated His-159 and the thiolate sulfur of the TSC moiety, as shown in Fig. 6. In addition to this strong H-bond, weak non-conventional H-bonds of the form C-H···S between the TSC moiety and His-159, as well as C-H···N between the TSC moiety and Cys-25 have been revealed in the complexes 1a-1d. Although these non-conventional H-bonds are weak since $\rho(r_{BCP}) \ll 0.1$ a.u., the average E_{int} value is -1.653 kcal/mol and $-V(r_{BCP})/G(r_{BCP}) < 1$, their additive effect is quite noticeable and can play an important role in inhibitor-active site binding. In each of the complexes 2a-2d, QTAIM analysis has shown the existence of moderately strong H-bonds of the form S-H···N and N-H···N between the TSC moiety and His-159 (with $\rho(r_{BCP}) \simeq 0.02$ a.u., an average E_{int} value -4.221 kcal mol^{-1} and $1 < -V(r_{BCP})/G(r_{BCP}) < 2$), and weak H-bonds of the form C-H···S and N-H···S among

Table 3. The Electron Density [$\rho(r_{BCP})$], its Laplacian [$\nabla^2\rho(r_{BCP})$], Kinetic Energy Density [$G(r_{BCP})$], Potential Energy Density [$V(r_{BCP})$], Energy Density [$H(r_{BCP})$] at the BCP, and Interatomic Interaction Energies (E_{int}) for the Noncovalent and Thiocarbonyl Carbon-thiolate Sulfur Bonding Interactions in 1a-1d

Complex	Intermolecular interaction	$\rho(r_{BCP})$ (a.u.)	$\nabla^2\rho(r_{BCP})$ (a.u.)	$V(r_{BCP})$ (a.u.)	$G(r_{BCP})$ (a.u.)	$-V(r_{BCP})/G(r_{BCP})$	$H(r_{BCP})$ (a.u.)	E_{int} (kcal mol^{-1})
1a	C3-S29	0.1144	-0.0671	-0.0881	0.0357	2.4708	-0.0524	-27.640
	C45-H50···S5	0.0078	0.0241	-0.0043	0.0052	0.8348	0.0009	-1.352
	N39-H56···S5	0.0346	0.0325	-0.0242	0.0162	1.4970	-0.0080	-7.590
	C44-H51···S5	0.0052	0.0152	-0.0026	0.0032	0.8045	0.0006	-0.803
	C30-H38···N1	0.0135	0.0397	-0.0089	0.0094	0.9481	0.0005	-2.806
	Im(N41)···(C12)Ph[a]	0.0075	0.0244	-0.0042	0.0052	0.8186	0.0009	-1.329
	N1=C6···H34-N32	0.0075	0.0193	-0.0043	0.0045	0.9367	0.0003	-1.334
	C9-H21···H34-N32	0.0051	0.0159	-0.0027	0.0033	0.8059	0.0006	-0.841
	N32-H35···H25-C7	0.0053	0.0193	-0.0030	0.0039	0.7721	0.0009	-0.950
1b	C3–S25	0.1157	-0.0705	-0.0894	0.0359	2.4905	-0.0535	-28.062
	C41–H46···S5	0.0078	0.0240	-0.0043	0.0051	0.8339	0.0009	-1.347
	N35–H52···S5	0.0352	0.0318	-0.0246	0.0163	1.5121	-0.0083	-7.729
	C40–H47···S5	0.0053	0.0154	-0.0026	0.0032	0.8062	0.0006	-0.813
	C26–H34···N1	0.0135	0.0399	-0.0090	0.0095	0.9477	0.0005	-2.821
	Im(N37)···(C12)Ph*	0.0075	0.0248	-0.0043	0.0052	0.8188	0.0010	-1.347
	N1=C6···H30-N28	0.0071	0.0182	-0.0040	0.0043	0.9300	0.0003	-1.241
	C9-H16···H30-N28	0.0043	0.0140	-0.0022	0.0029	0.7729	0.0006	-0.694
1c	C3-S32	0.1142	-0.0664	-0.0879	0.0357	2.4657	-0.0523	-27.583
	C48-H53···S5	0.0079	0.0243	-0.0044	0.0052	0.8364	0.0009	-1.373
	N42-H59···S5	0.0346	0.0325	-0.0242	0.0162	1.4968	-0.0080	-7.592
	C47-H54···S5	0.0053	0.0154	-0.0026	0.0032	0.8079	0.0006	-0.819
	C33-H41···N1	0.0133	0.0393	-0.0088	0.0093	0.9460	0.0005	-2.770
	Im(N44)···(C13)Ph[a]	0.0075	0.0245	-0.0042	0.0052	0.8174	0.0009	-1.326
	N1=C6···H37-N35	0.0076	0.0196	-0.0043	0.0046	0.9402	0.0003	-1.362
	C10-H22···H37-N35	0.0052	0.0161	-0.0028	0.0034	0.8134	0.0006	-0.866

Table 3. Continued

1d	C3-S28	0.1157	-0.0706	-0.0895	0.0359	2.4909	-0.0536	-28.085
	C44-H49···S5	0.0079	0.0242	-0.0043	0.0052	0.8347	0.0009	-1.357
	N38-H55···S5	0.0355	0.0316	-0.0250	0.0164	1.5190	-0.0085	-7.830
	C43-H50···S5	0.0053	0.0154	-0.0026	0.0032	0.8066	0.0006	-0.818
	C29-H37···N1	0.0132	0.0392	-0.0088	0.0093	0.9440	0.0005	-2.750
	Im(N40)···(C13)Ph[a]	0.0075	0.0247	-0.0043	0.0052	0.8167	0.0010	-1.338
	N1=C6···H33-N31	0.0074	0.0190	-0.0042	0.0045	0.9384	0.0003	-1.316

[a]Im and Ph represent the imidazole and phenyl rings, respectively, indicating that the atoms in parentheses are part of the respective rings

the TSC moiety and the active site residues of FP2 (with $\rho(r_{BCP}) \ll 0.1$ a.u., an average E_{int} value -1.381 kcal mol^{-1}, and $-V(r_{BCP})/G(r_{BCP}) < 1$). The concerted action of the covalent and noncovalent interactions in the inhibitor-FP2 active site complexes studied can enable the TSC-based inhibitors bind specifically but momentarily to the active site residues of FP2. It is worthy of note that QTAIM analysis has confirmed the intermolecular interactions in the complexes that were earlier predicted by structural analysis based on geometrical cutoff limits, and has also elucidated several interactions that could not be identified by structural analysis alone.

In the complexes 1a-1d, there exist the noncovalent interactions: Imidazole ring···Phenyl ring (demarcated by the red circle in Fig. 6) and N=C···H-N between the TSC moiety and the active site residues of FP2, which are indicative of π-stacking and N-H···π interactions respectively. These interactions further strengthen the binding between the inhibitor and the active site, thereby providing extra stability to the complexes of series 1 as compared to those of series 2 in which π-stacking and N-H···π interactions are not observed. It is clear from Fig. 6 that nearly all complexes of series 1 are further stabilized by an H-H interaction between one hydrogen atom of the terminal NH_2 group of Cys-25 and one phenyl hydrogen of the TSC-based inhibitor.

Noncovalent interaction (NCI) index analysis

To adequately describe the subtle interplay of attractive (bonding) and repulsive (non-bonding) noncovalent interactions in the inhibitor-FP2 active site complexes studied, the foregoing Barder's QTAIM analysis has been supplemented with the noncovalent interaction (NCI) index [47]. The NCI analysis is very useful in assessing how complementary the inhibitor and the active site are, and the extent to which weak interactions contribute to the stability of the inhibitor-FP2 active site complexes studied. In fact, a detailed understanding of the different noncovalent interactions in biomolecules is essential for the rational design of new drugs, since these interactions (especially those involving π-systems in general and aromatic rings in particular) are very relevant in supramolecular chemistry [48]. The NCI index methodology is very robust in characterizing (identifying and classifying) the noncovalent interactions in molecular systems based on a function of electron density ρ(r) and its first derivative ∇ρ(r) known as the reduced density gradient (RDG or s(r)) [49,50]:

$$s(r) = \frac{1}{2(3\pi^2)^{1/3}} \frac{|\nabla\rho(r)|}{\rho(r)^{4/3}}$$

The BCPs corresponding to noncovalent interactions with poor directionality are sometimes controversially excluded by the stringent QTAIM criterion of only analyzing electron density critical points. Interestingly, the NCI index transcends QTAIM by revealing noncovalent interactions in regions where QTAIM-defined BCPs are absent. The NCI index analysis elucidates noncovalent

Table 4. The Electron Density [$\rho(r_{BCP})$], its Laplacian [$\nabla^2\rho(r_{BCP})$], Kinetic Energy Density [$G(r_{BCP})$], Potential Energy Density [$V(r_{BCP})$], Energy Density [$H(r_{BCP})$] at the BCP, and Interatomic Interaction Energies (E_{int}) for the Noncovalent and Thiocarbonyl Carbon-thiolate Sulfur Bonding Interactions in 2a-2d

Complex	Intermolecular interaction	$\rho(r_{BCP})$ (a.u.)	$\nabla^2\rho(r_{BCP})$ (a.u.)	$V(r_{BCP})$ (a.u.)	$G(r_{BCP})$ (a.u.)	$-V(r_{BCP})/G(r_{BCP})$	$H(r_{BCP})$ (a.u.)	E_{int} (kcal mol^{-1})
2a	C3-S30	0.1180	-0.0692	-0.0875	0.0351	2.4928	-0.0524	-27.451
	S5-H29···N40	0.0156	0.0421	-0.0107	0.0106	1.0032	-0.0001	-3.323
	N4-H27···N40	0.0218	0.0498	-0.0161	0.0143	1.1281	-0.0018	-5.051
	C45-H52···S5	0.0063	0.0196	-0.0033	0.0041	0.8019	0.0008	-1.028
	N33-H36···S5	0.0101	0.0277	-0.0055	0.0062	0.8826	0.0007	-1.719
2b	C3-S26	0.1185	-0.0705	-0.0880	0.0352	2.5005	-0.0528	-27.612
	S5-H25···N36	0.0159	0.0425	-0.0108	0.0107	1.0082	-0.0001	-3.389
	N4-H23···N36	0.0221	0.0501	-0.0164	0.0144	1.1335	-0.0019	-5.139
	C41-H48···S5	0.0064	0.0194	-0.0032	0.0041	0.7997	0.0008	-1.016
	N29-H32···S5	0.0101	0.0278	-0.0055	0.0062	0.8824	0.0007	-1.723
2c	C3-S33	0.1177	-0.0686	-0.0873	0.0351	2.4885	-0.0522	-27.403
	S5-H32···N43	0.0156	0.0420	-0.0106	-0.0106	-1.0000	-0.0211	-3.313
	N4-H30···N43	0.0218	0.0498	-0.0161	0.0143	1.1287	-0.0018	-5.059
	C48-H55···S5	0.0065	0.0199	-0.0034	0.0042	0.8059	0.0008	-1.056
	N36-H39···S5	0.0102	0.0279	-0.0055	0.0062	0.8836	0.0007	-1.730
2d	C3-S29	0.1184	-0.0700	-0.0879	0.0352	2.4967	-0.0527	-27.593
	S5-H28···N39	0.0158	0.0424	-0.0108	0.0107	1.0071	-0.0001	-3.371
	N4-H26···N39	0.0220	0.0500	-0.0163	0.0144	1.1327	-0.0019	-5.122
	C44-H51···S5	0.0064	0.0197	-0.0033	0.0041	0.8027	0.0008	-1.038
	N32-H35···S5	0.0102	0.0280	-0.0055	0.0063	0.8835	0.0007	-1.737

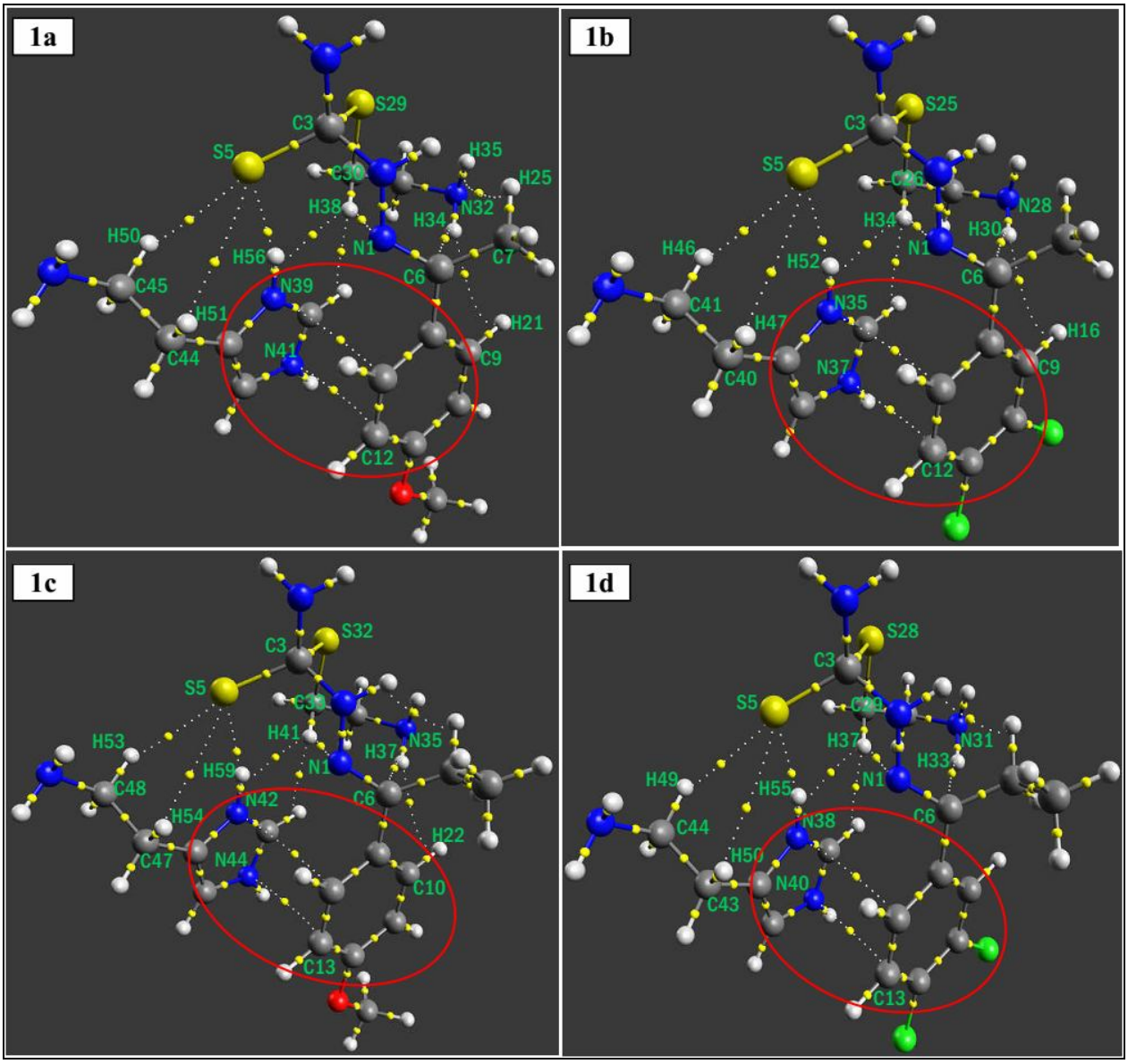

Fig. 6. Molecular graphs of the complexes of series 1 plotted using Avogadro 1.1.1; the tiny yellow spheres and the white dashed lines represent bond critical points and bond paths, respectively. The ring critical points have been excluded for clarity.

interactions by means of colored isosurfaces obtained by mapping sign(λ_2)ρ(r) onto a 3-dimensional RDG isosurface, based on a red-yellow-green-blue color code: blue for attractive interactions, yellow and green for weak repulsive and weak attractive interactions respectively, and red for steric repulsion [48,49,51]. The NCI index analysis utilizes the sign of the second eigenvalue of the electron-density Hessian matrix (λ_2) to distinguish between attractive or bonding interactions ($\lambda_2 < 0$) and repulsive or non-bonding interactions ($\lambda_2 > 0$) [51,52]. The RDG-based NCI isosurfaces of the complexes of both series 1 and 2 currently studied are depicted in Figs. 8 and 9, respectively, as

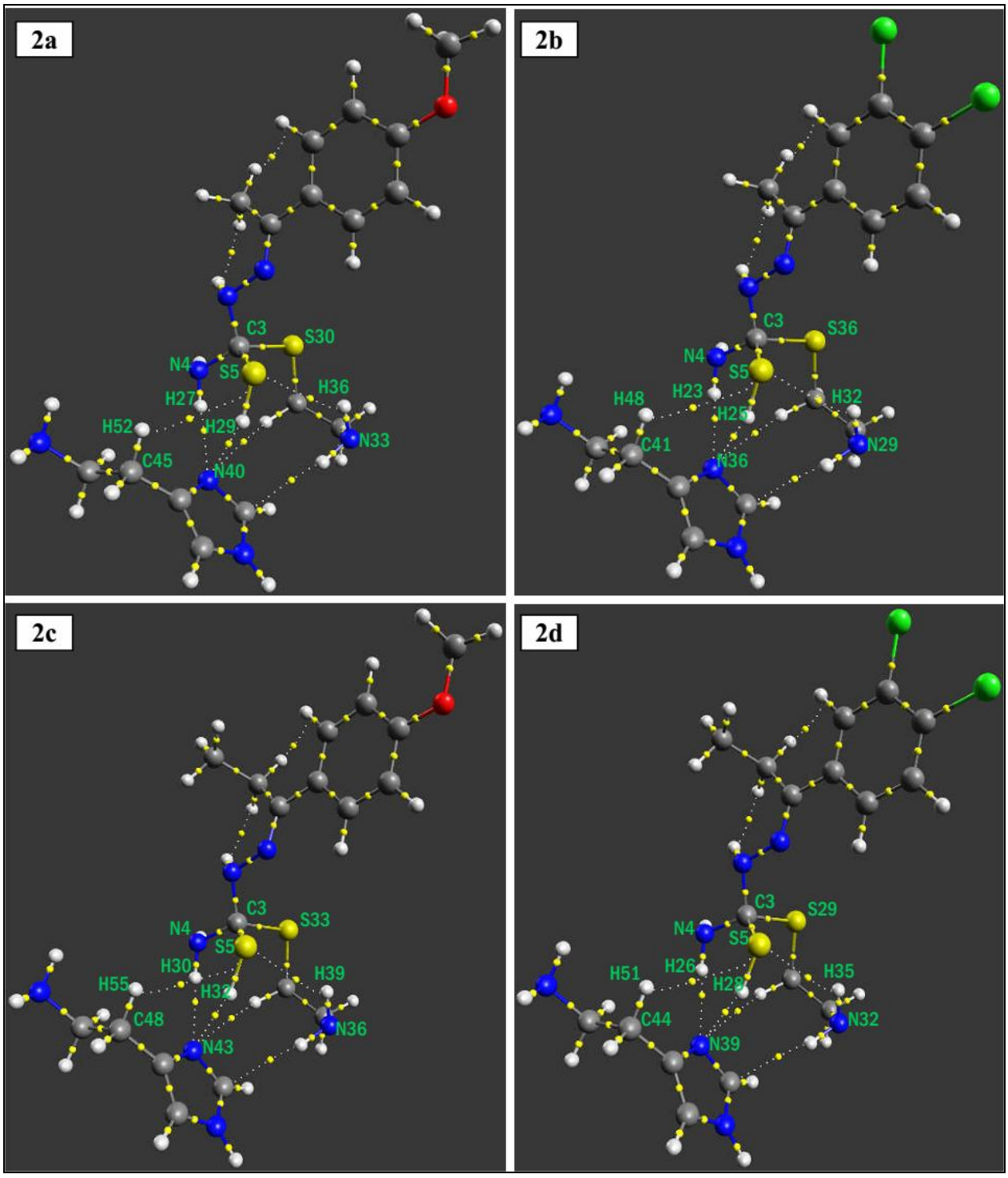

Fig. 7. Molecular graphs of the complexes of series 2 plotted using Avogadro 1.1.1; the tiny yellow spheres and the white dashed lines represent bond critical points and bond paths, respectively. The ring critical points have been excluded for clarity.

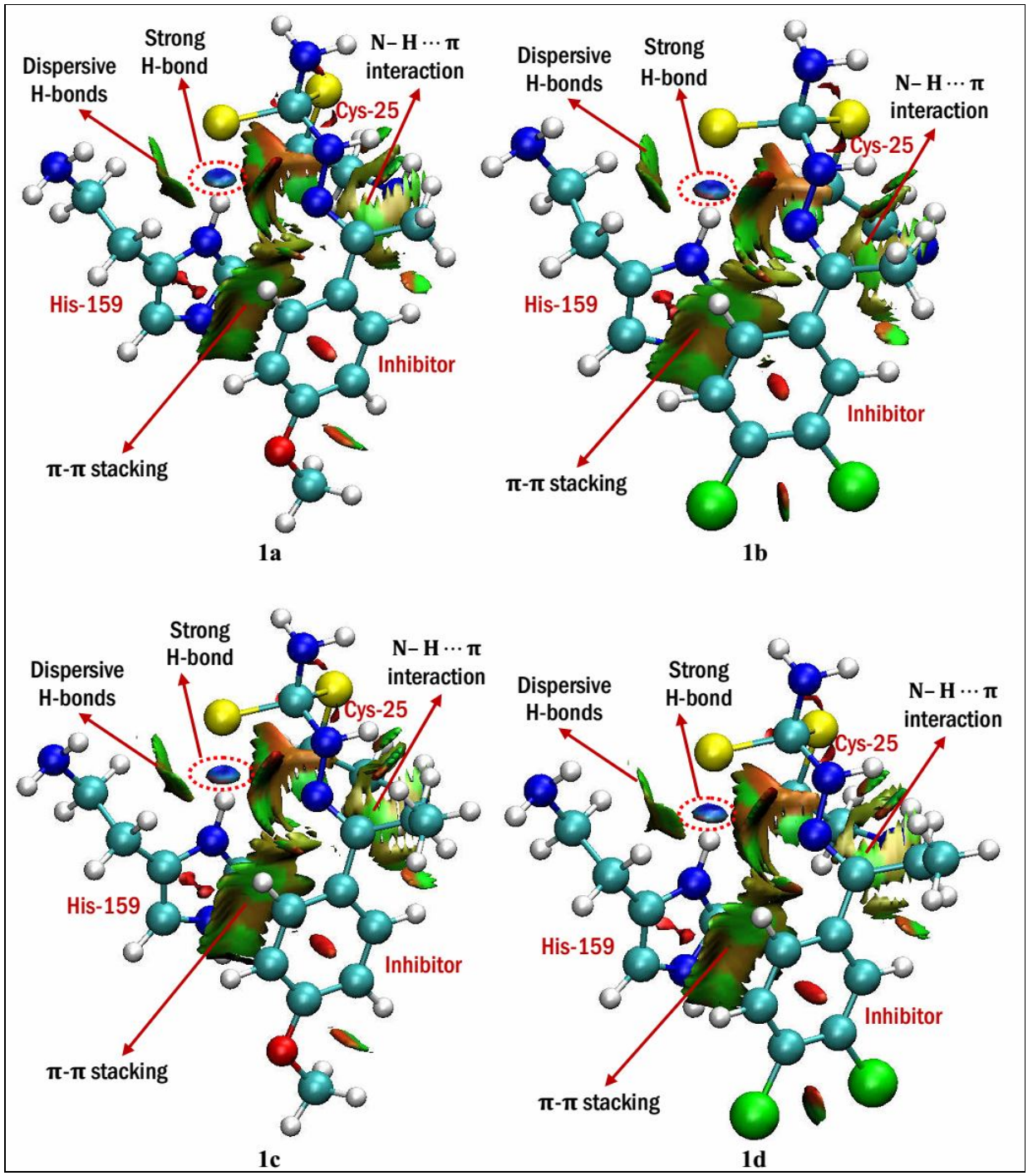

Fig. 8. NCI isosurfaces of the complexes of series 1 generated by Multiwfn 3.3.9 for s(r) = 0.05 a.u., and visualized by VMD 1.9.3. The isosurfaces are colored on a red-yellow-green-blue scale according to the values of sign(λ2)ρ(r), ranging from -0.05 to 0.05 a.u. Blue indicates strong attractive interactions and red indicates strong non-bonded overlap.

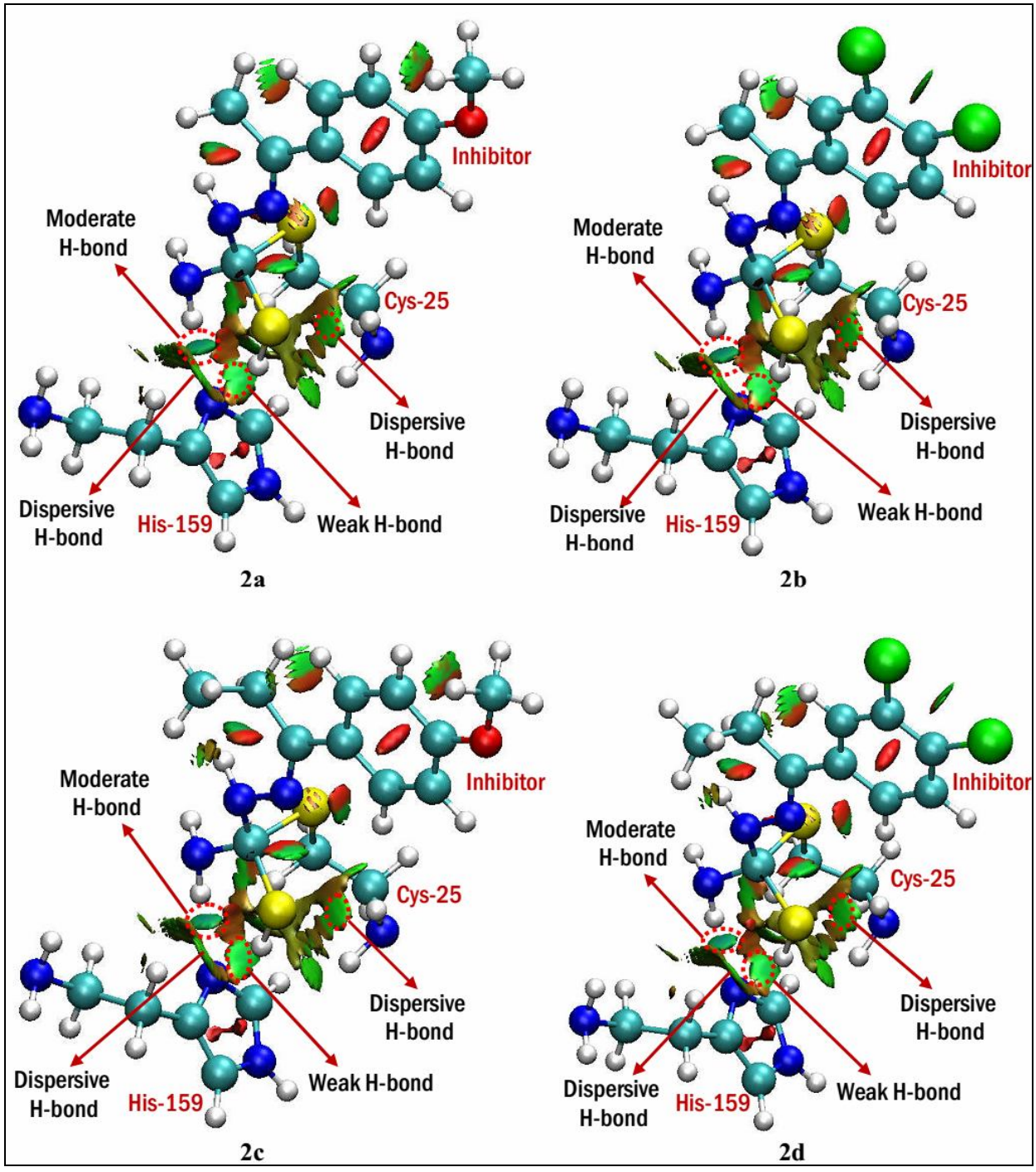

Fig. 9. NCI isosurfaces of the complexes of series 2 generated by Multiwfn 3.3.9 for s(r) = 0.05 a.u., and visualized by VMD 1.9.3. The isosurfaces are colored on a red-yellow-green-blue scale according to the values of sign(λ2)ρ(r), ranging from -0.05 to 0.05 a.u. Blue indicates strong attractive interactions and red indicates strong non-bonded overlap.

visualized in 3-dimensional space using VMD 1.9.3.

In Figs. 8 and 9, only the interactions between the TSC-based inhibitor molecules and the active site residues of FP2 are labeled. As evidenced from these figures, all noncovalent interactions revealed by QTAIM analysis have been confirmed by the NCI isosurfaces. Strong H-bonds of the form N-H···S between the hydrogen atom attached to the epsilon-nitrogen of the imidazole ring in protonated His-159 and the thiolate sulfur of the TSC moiety in each complex of series 1, is clearly elucidated by a blue colored disc-shaped isosurface. It is clear from the NCI isosurfaces that the weak non-conventional H-bonds C-H···S between the TSC moiety and the His-159 residue, as well as C-H···N between the TSC moiety and Cys-25 in the complexes of series 1, are dispersive in nature. The existence of π-stacking interactions between the imidazole and phenyl rings in the complexes 1a-1d is validated by the presence of a large and almost flat isosurface in the region between these rings. The N-H···π interaction in each of these complexes is also revealed by an NCI isosurface between the NH_2 group of Cys-25 and the azomethine group of the TSC moiety.

In the complexes 2a-2d, the NCI index analysis has revealed moderately strong H-bonds of the form N-H···N and weak H-bonds of the form S-H···N via light-blue and green colored isosurfaces, respectively, between the TSC moiety and the His-159 residue. Furthermore, weak dispersive-like H-bonds of the form C-H···S and N-H···S among the TSC moiety and the active site residues of FP2 are also elucidated *via* NCI isosurfaces. Unlike the complexes of series 1, NCI isosurfaces for π-staking and N-H···π interactions are not evidenced in the complexes 2a-2d.

CONCLUSIONS

Thiosemicarbazones (TSCs) possess significant antimalarial properties that are believed to be linked to the inhibition of major cysteine proteases (such falcipain-2) in *Plasmodium falciparum*, but the binding modes of TSCs to the active site of these enzymes are unclear. In an effort to provide a detailed insight into the nature of the bonding interactions between the active site of falcipain-2 and TSC-based inhibitors, different derivatives of acetophenone thiosemicarbazone (APTSC) and propiophenone thiosemicarbazone (PPTSC) have been chosen as illustrative examples. These choices have been made because APTSC and PPTSC derivatives are known to possess inhibitory effects against *Plasmodium falciparum*. The equilibrium geometries of the inhibitor-active site complexes in the aqueous phase have been obtained via dispersion-corrected density functional theory calculations at RI-BP86-D3(BJ)/def2-TZVP level of theory. Thereafter, an in-depth analysis of the covalent and noncovalent interactions in these complexes has been performed in the framework of the quantum theory of atoms in molecules (QTAIM) and the noncovalent interaction (NCI) index, at RIJCOSX-M06-2X/def2-TZVPP level of theory.

Our results have revealed both covalent and noncovalent interactions between the TSC-based inhibitors and the active site residues (Cys-25 and His-159) of falcipain-2. In each complex, the covalent interaction exists between the thiocarbonyl carbon of the TSC moiety and thiolate sulfur of the active site cysteine (Cys-25) residue of falcipain-2. A subtle interplay of noncovalent interactions such as hydrogen bonds, dispersive-like van der Waals and π-stacking interactions have been elucidated between the TSC moieties of the inhibitors and the active site residues of the enzyme. Prominent among the noncovalent interactions are sulfur-centered hydrogen bonds formed between the TSC moieties of the inhibitors and the histidine (His-159) residue of the active site. The synergy of these covalent and noncovalent interactions enables the TSCs studied herein to bind specifically but transiently to the active site residues of falcipain-2. Based on our results, APTSC and PPTSC derivatives are potential covalent reversible inhibitors of falcipain-2, and are therefore promising precursor for the manufacture of antimalarial drugs.

ACKNOWLEDGEMENTS

This work has been supported by the Ministry of Higher Education of Cameroon through the research modernization allowance offered to faculty members, which we gratefully acknowledge.

REFERENCES

[1] Adams, M.; Barnard, L.; Carmen de Kock; Smith, P. J.; Wiesner, L.; Chibale, K.; Smith, G. S.,

Cyclopalladated organosilane-tethered thiosemicarbazones: novel strategies for improving antiplasmodial activity. *Dalton Trans.* **2016**, *45*, 5514-5520, DOI: 10.1039/c5dt04918k.

[2] Pandey, K. C.; Wang, S. X.; Sijwali, P. S.; Lau, A. L.; McKerrow, J. H.; Rosenthal, P. J., The Plasmodium falciparum cysteine protease falcipain-2 captures its substrate, hemoglobin, *via* a unique motif. *Proc. Natl. Acad. Sci.* **2005**, *102*, 9138-9143, DOI: 10.1073/pnas. 0502368102.

[3] Navarro, M.; Gabbiani, C.; Messori, L.; Gambino, D., Metal-based drugs for malaria, trypanosomiasis and leishmaniasis: recent achievements and perspectives. *Drug. Discov. Today.* **2010**, *15*, 1070-1078, DOI: 10.1016/j.drudis.2010.10.005.

[4] Fatondji, H. R.; Kpoviessi, S.; Gbaguidi F.; Bero J.; Hannaert V.; Quetin-Leclercq J.; Poupaert J.; Moudachirou M.; Accrombessi G. C., Structure-activity relationship study of thiosemicarbazones on an African trypanosome: Trypanosoma brucei brucei. *Med. Chem. Res.* **2013**, *22*, 2151-2162, DOI: 10.1007/s00044-012-0208-6.

[5] Ghogomu J. N.; Nkungli. N. K., A DFT study of some structural and spectral properties of 4-methoxyacetophenone thiosemicarbazone and its complexes with some transition metal chlorides: potent antimicrobial agents. Advances in Chemistry. 2016, Volume 2016, Article ID 9683630, 15 pages, http://dx.doi.org/10.1155/2016/9683630.

[6] Adams, M.; Carmen de Kock; Smith, P. J.; Chibale, K.; Smith G. S., Synthesis, characterization and antiplasmodial evaluation of cyclopalladated thiosemicarbazone complexes. *J.Organomet . Chem.*, **2013**, *736*, 19-26, DOI: 10.1016/ j.jorganchem.2013.02.024.

[7] Chellan, P.; Land, K. M.; Shokar, A.; Au, A.; An, S. H.; Clavel, C. M.; Dyson, P. J.; Carmen de Kock; Smith, P. J.; Chibale, K.; Smith, G. S., Exploring the versatility of cycloplatinated thiosemicarbazones as antitumor and antiparasitic agents. *Organometallics.* **2012**, *31*, 5791-5799, DOI: dx.doi.org/ 10.1021/ om300334z.

[8] Pandey, K. C., Cysteine proteases of human malaria parasites. *J. Parasit. Dis.* **2011**, *35*, 94-103, DOI: 10.1007/s12639-011-0084-x.

[9] Quesne, M. G.; Ward, R. A.; De Visser, S. P., Cysteine protease inhibition by nitrile-based inhibitors: a computational study. *Front. Chem.* **2013**, *1*, 1-10, DOI: 10.3389/fchem. 2013.00039.

[10] Trossini, G. H. G.; Guido, R. V. C; Oliva, G.; Ferreira, E. I.; Andricopulo, A. D., Quantitative structure-activity relationships for a series of inhibitors of cruzain from Trypanosoma cruzi: molecular modeling, CoMFA and CoMSIA studies. *J. Mol. Graph. Model.* **2009**, *28*, 3-11, DOI: 10.1016/ j.jmgm.2009.03.001.

[11] Hempelmann, E., Hemozoin biocrystallization in Plasmodium falciparum and the antimalarial activity of crystallization inhibitors. *Parasitol. Res.* **2007**, *100*, 671-676, DOI: 10.1007/ s00436-006-0313-x.

[12] Tsipis, A. C., DFT flavor of coordination chemistry. *Coord. Chem. Rev.* **2014**, *272*, 1-29, DOI: 10.1016/ j.ccr.2014.02.023.

[13] Risthaus, T.; Grimme, S., Benchmarking of London dispersion-accounting density functional theory methods on very large molecular complexes. *J. Chem. Theory Comput.* **2013**, *9*, 1580-1591, DOI: 10.1021/ ct301081n.

[14] Fricker, S. P., Cysteine proteases as targets for metal-based drugs. *Metallomics.* **2010**, *2*, 366-377, DOI: 10.1039/b924677k.

[15] Neese, F., The ORCA program system. Wiley Interdiscip. *Rev. Comput. Mol. Sci.* **2012**, *2*, 73-78, DOI: 10.1002/wcms.81.

[16] Humphrey, W.; Dalke, A.; Schulten, K., VMD: visual molecular dynamics. *J. Mol. Graphics Modell.* **1996**, *14*, 33-38, DOI: 10.1016/0263-7855(96)00018-5.

[17] Vernet, T.; Tessier, D. C.; Chatellier, J.; Plouffe, C.; Lee, T. S.; Thomas, D. Y.; Storer, A. C.; Ménard, R., Structural and functional roles of asparagine 175 in the cysteine protease papain. *J. Biol. Chem.* **1995**, *270*, 16645-16652, DOI: 10.1074/jbc.270.28.16645.

[18] Becke, A. D., Density-functional exchange-energy approximation with correct asymptotic behavior. *Phys. Rev. A.* **1988**, *38*, 3098-3100, DOI: 10.1103/ PhysRevA.38. 3098.

[19] Perdew, J. P., Density-functional approximation for the correlation energy of the inhomogeneous electron

gas. *Phys. Rev. B.* **1986**, *34*, 8822-8824, DOI: 10.1103/PhysRevB. 33.8822.

[20] Grimme, S.; Ehrlich, S.; Goerigk, L., Effect of the damping function in dispersion corrected density functional theory. *J. Comp. Chem.* **2011**, *32*, 1456-1465, DOI: 10.1002/jcc.21759.

[21] Keith, T. A., AIMAll (Version 16.01.09); TK Gristmill Software: Overland Park KS, USA, 2016, www. aim.tkgristmill.com.

[22] Lu, T.; Chen, F. W., Multiwfn: A multifunctional wavefunction analyzer. *J. Comput. Chem.* **2012**, *33*, 580-592, DOI: 10.1002/jcc.22885.

[23] Hanwell, M. D.; Curtis, D. E.; Lonie, D. C.; Vandermeersch, T.; Zurek, E.; Hutchison, G. R., Avogadro: An advanced semantic chemical editor, visualization, and analysis platform. *J. Cheminform.* **2012**, *4*, 1-17, DOI: 10.1186/1758-2946-4-17.

[24] Marenich A. V.; Cramer C. J.; Truhlar D. G., Universal solvation model based on solute electron density and on a continuum model of the solvent defined by the bulk dielectric constant and atomic surface tensions. *J. Phys. Chem. B.* **2009**, *113*, 6378-6396, DOI: 10.1021/jp810292n.

[25] Neese, F., An improvement of the resolution of the identity approximation for the calculation of the coulomb matrix. *J. Comp. Chem.* **2003**, *24*, 1740-1747, DOI: 10.1002/jcc.10318.

[26] Neese, F.; Wennmohs, F.; Hansen, A.; Becker, U., Efficient, approximate and parallel Hartree-Fock and hybrid DFT calculations. A 'chain-of-spheres' algorithm for the Hartree-Fock exchange. *Chem. Phys.* **2009**, *356*, 98-109, DOI: 10.1016/ j.chemphys.2008.10.036.

[27] Goerigk, L.; Grimme, S., A thorough benchmark of density functional methods for general main group thermochemistry, kinetics, and noncovalent interactions. *Phys. Chem. Chem. Phys.* **2011**, *13*, 6670-6688, DOI: 10.1039/C0CP02984J.

[28] Sweeney, D.; Raymer, M. L.; Lockwood, T. D., Antidiabetic and antimalarial biguanide drugs are metal-interactive antiproteolytic agents. *Biochem. Pharmacol.* **2003**, *66*, 663-677, DOI: 10.1016/S0006-2952(03)00338-1.

[29] Jeffrey, G. A., An Introduction to Hydrogen Bonding. Oxford University Press, 1997.

[30] Biswal, H. S., Hydrogen bonds involving sulfur: New insights from ab initio calculations and gas phase laser spectroscopy, in: S. Scheiner (Ed.), Noncovalent forces. Springer, 2015, p. 15-24.

[31] van Bergen, L. A. H.; Alonso, M.; Palló, A.; Nilsson, L.; De Proft F.; Messens J., Revisiting sulfur H-bonds in proteins: The example of peroxiredoxin AhpE. *Sci. Rep.* **2016**, *6*, 30369-30379, DOI: 10.1038/srep30369.

[32] Schalley, C. A., Noncovalent Bonding in Supramolecular Chemistry, in: Schalley, C. A. (Ed.), Analytical Methods in Supramolecular Chemistry. WILEY-VCH Verlag GmbH & Co. KGaA, Weinheim, 2007, p. 1-16.

[33] Steiner, T., The hydrogen bond in the solid state. *Angew. Chem. Int. Ed.* **2002**, *41*, 48-76, DOI: 10.1002/1521-3773(20020104)41:1<48::AID-ANIE48>3.0.CO;2-U.

[34] Zhao, Y.; Truhlar, D. G., The M06 suite of density functionals for main group thermochemistry, thermochemical kinetics, noncovalent interactions, excited states, and transition elements: two new functionals and systematic testing of four M06-class functionals and 12 other functional. *Theor. Chem. Account.* **2008**, *120*, 215-241, DOI 10.1007/s00214-007-0310-x.

[35] Becke, A. D., Density-functional thermochemistry. III. The role of exact exchange. *J. Chem. Phys.* **1993**, *98*, 5648-5652, DOI: 10.1063/1.464913.

[36] Lee, C. T.; Yang, W. T.; Parr, R. G., Development of the colle-salvetti correlation-energy formula into a functional of the electron-density. *Phys. Rev. B: Condens. Matter Mater. Phys.* **1988**, *37*, 785-789, DOI: 10.1103/PhysRevB.37.785.

[37] Bader, R. F. W., Atoms in molecules. A Quantum Theory, Oxford University Press, Oxford, 1990.

[38] Matta, C. F.; Boyd, R. J., An Iintroduction to the Quantum Theory of Atoms in Molecules, in: Matta, C. F.; Boyd, R. J. (Eds.), The quantum theory of atoms in molecules. WILEY-VCH Verlag GmbH & Co. KGaA, Weinheim, 2007, p. 1-34.

[39] Singh, R. N.; Rawat, P., Spectral analysis, structural elucidation, and evaluation of both nonlinear optical properties and chemical reactivity of a newly

synthesized ethyl-3,5-dimethyl-4-[(toluenesulfonyl)-hydrazonomethyl]-1H-pyrrole-2-carboxylate through experimental studies and quantum chemical calculations. *J. Mol. Struct.* **2013**, *1054-1055*, 65-75, DOI: 10.1016/j.molstruc.2013.09.034.

[40] Trendafilova, N.; Bauer, G.; Mihaylov T., DFT and AIM studies of intramolecular hydrogen bonds in dicoumarols. Chem. Phys. **2004**, 302, 95-104, DOI: 10.1016/j.chemphys.2004.03. 021.

[41] Baryshnikov, G. V.; Minaev, B. F.; Minaeva, V. A.; Podgornaya, A. T.; Ågren, H., Application of Bader's atoms in molecules theory to the description of coordination bonds in the complex compounds of Ca^{2+} and Mg^{2+} with Methylidene Rhodanine and its anion. *Russ. J. Gen. Chem.* **2012**, *82*, 1254-1262, DOI: 10.1134/S1070363212070122.

[42] Cremer, D.; Kraka, E., Theoretical determination of molecular structure and conformation. 15. three-membered rings: bent bonds, ring strain, and surface delocalization. *J. Am. Chem. Soc.* **1985**, *107*, 3800-3810, DOI: 10.1021/ja00299a009.

[43] Ebrahimi, A.; Razmazma, H.; Delarami, H. S., The nature of halogen bonds in $[N\cdots X\cdots N]^+$ complexes: A theoretical study. *Phys. Chem. Res.* **2016**, *4*, 1-15, DOI: 10.22036/pcr. 2016.11619.

[44] Du, J.; Sun, X.; Jiang, G., Exploring the interaction natures in plutonyl(VI) complexes with topological analyses of electron density. *Int. J. Mol. Sci.* **2016**, *17*, 414-426; DOI: 10.3390/ijms17040414.

[45] Koch, U.; Popelier, P. L. A., Characterization of C-H-O hydrogen bonds on the basis of the charge density. *J. Phys. Chem.* **1995**, *99*, 9747-9754, DOI: 10.1021/j100024a016.

[46] Espinosa, E.; Molins, E.; Lecomte, C., Hydrogen bond strengths revealed by topological analyses of experimentally observed electron densities. *Chem. Phys. Lett.* **1998**, *285*, 170-173, DOI: 10.1016/S0009-2614(98)00036-0.

[47] Johnson, E. R.; Keinan, S.; Mori-Sanchez, P.; Contreras-Garcia, J.; Cohen, A. J.; Yang, W., Revealing noncovalent interactions. *J. Am. Chem. Soc.* **2010**, *132*, 6498-6506, DOI: 10.1021/ja100936w.

[48] Bauzá, A.; Quiñonero, D.; Frontera, A.; Ballester, P., Reconciling experiment and theory in the use of aryl-extended calix[4]pyrrole receptors for the experimental quantification of chloride-π interactions in solution. *Int. J. Mol. Sci.* **2015**, *16*, 8934-8948, DOI: 10.3390/ ijms16048934.

[49] Contreras-García, J.; Boto, R. A.; Izquierdo-Ruiz, F.; Reva, I.; Woller, T.; Alonso, M., A benchmark for the non□covalent interaction (NCI) index or… is it really all in the geometry? *Theor. Chem. Acc.* **2016**, *135*, 242-255, DOI: 10.1007/s00214-016-1977-7.

[50] Wu, P.; Chaudret, R.; Hu, X.; Yang, W., Noncovalent interaction analysis in fluctuating environments. *J. Chem. Theory Comput.* **2013**, *9*, 2226-2234, DOI: 10.1021/ct4001087.

[51] Saleh, G.; Gatti, C.; Presti, L. L.; Contreras-García, J., Revealing noncovalent interactions in molecular crystals through their experimental electron densities. *Chem. Eur. J.* **2012**, *18*, 15523-15536, DOI: 10.1002/chem.201201290.

[52] Contreras-García, J.; Johnson, E. R.; Keinan, S.; Chaudret, R.; Piquemal, J. -P.; Beratan, D. N.; Yang, W., NCIPLOT: a program for plotting noncovalent interaction regions. *J. Chem. Theory Comput.* **2011**, *7*, 625-632, DOI: 10.1021/ct100641a.